Article

Quantum Effects on Hydrogen Isotope Adsorption on Single-Wall Carbon Nanohorns

Hideki Tanaka, Hirofumi Kanoh, Masako Yudasaka, Sumio Iijima, and Katsumi Kaneko

J. Am. Chem. Soc., **2005**, 127 (20), 7511-7516• DOI: 10.1021/ja0502573 • Publication Date (Web): 28 April 2005

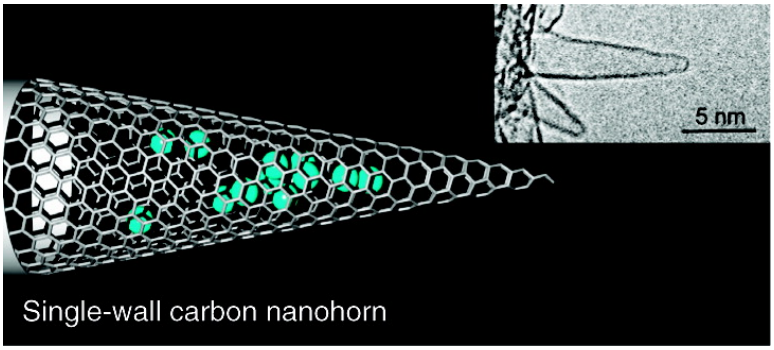

More About This Article

Additional resources and features associated with this article are available within the HTML version:

- Supporting Information
- Links to the 22 articles that cite this article, as of the time of this article download
- Access to high resolution figures
- Links to articles and content related to this article
- Copyright permission to reproduce figures and/or text from this article

View the Full Text HTML

J|A|C|S
ARTICLES
Published on Web 04/28/2005

Quantum Effects on Hydrogen Isotope Adsorption on Single-Wall Carbon Nanohorns

Hideki Tanaka,[†] Hirofumi Kanoh,[‡] Masako Yudasaka,[§,¶] Sumio Iijima,[§,¶,#] and Katsumi Kaneko*[,‡]

Contribution from the Diversity and Fractal Science, Graduate School of Science and Technology, Chiba University, 1-33 Yayoi, Inage, Chiba 263-8522, Japan, Department of Chemistry, Faculty of Science, Chiba University, 1-33 Yayoi, Inage, Chiba 263-8522, Japan, SORST, Japan Science and Technology Agency, c/o NEC Corporation, 34 Miyukigaoka, Tsukuba 305-8501, Japan, NEC Corporation, 34 Miyukigaoka, Tsukuba 305-8501, Japan, and Department of Physics, Meijo University, 1-501 Shiogamaguchi, Tenpaku, Nagoya 468-8502, Japan

Received January 14, 2005; E-mail: kaneko@pchem2.s.chiba-u.ac.jp

Abstract: H_2 and D_2 adsorption on single-wall carbon nanohorns (SWNHs) have been measured at 77 K, and the experimental data were compared with grand canonical Monte Carlo simulations for adsorption of these hydrogen isotopes on a model SWNH. Quantum effects were included in the simulations through the Feynman−Hibbs effective potential. The simulation predictions show good agreement with the experimental results and suggest that the hydrogen isotope adsorption at 77 K can be successfully explained with the use of the effective potential. According to the simulations, the hydrogen isotopes are preferentially adsorbed in the cone part of the SWNH with a strong potential field, and quantum effects cause the density of adsorbed H_2 inside the SWNH to be 8−26% smaller than that of D_2. The difference between H_2 and D_2 adsorption increases as pressure decreases because the quantum spreading of H_2, which is wider than that of D_2, is fairly effective at the narrow conical part of the SWNH model. These facts indicate that quantum effects on hydrogen adsorption depend on pore structures and are very important even at 77 K.

I. Introduction

Hydrogen adsorption in carbonaceous materials has received considerable attention in recent decades.[1−9] The hydrogen storage capacity of single-wall carbon nanotubes (SWNTs) and graphitic slit pores has often been investigated by simulating their hydrogen adsorption under the assumption that hydrogen can be modeled as a classical fluid above 77 K.[10−12] Wang et al., however, have recently developed a path-integral grand canonical Monte Carlo (PI-GCMC) technique to explore the statistical properties of quantum fluids[13] and have used PI-GCMC simulation to study hydrogen storage capacity of SWNTs and graphitic slit pores.[14] Surprisingly, they showed that even at 298 K quantum effects are important for adsorption in the interstices of SWNT bundles; the interstitial adsorption of hydrogen predicted by the quantum simulations is quite smaller than that predicted by classical simulations. Challa et al. used the PI-GCMC simulations to determine selectivities of hydrogen isotopes for SWNTs through quantum molecular sieving above 20 K[15,16] and found that the selectivity of tritium over hydrogen in the (10,10) nanotube interstice is extremely large at 20 K and is still significant at 77 K, even though quantum effects diminish dramatically as temperature increases. Darkrim et al.[17−19] investigated hydrogen adsorption on SWNTs at 293 and 77 K by using GCMC simulations with quantum effective potential derived from the Feynman−Hibbs (FH) perturbative approach.[20,21] They showed that the hydrogen adsorption at 298 K predicted by quantum simulations based on the FH effective potential is several percent smaller than

[†] Graduate School of Science and Technology, Chiba University.
[‡] Faculty of Science, Chiba University.
[§] Japan Science and Technology Agency.
[¶] NEC Corporation.
[#] Meijo University.

(1) Carpetis, C.; Peschka, W. *Int. J. Hydrogen Energy* **1980**, *5*, 539.
(2) Chahine, R.; Bose, T. K. *Int. J. Hydrogen Energy* **1994**, *19*, 161.
(3) Dillon, A. C.; Jones, K. M.; Bekkedahl, T. A.; Kiang, C. H.; Bethune, D. S.; Heben, M. J. *Nature* **1997**, *386*, 377.
(4) Liu, C.; Fan, Y. Y.; Liu, M.; Cong, H. T.; Cheng, H. M.; Dresselhaus, M. S. *Science* **1999**, *286*, 1127.
(5) Ye, Y.; Ahn, C. C.; Witham, C.; Fultz, B.; Liu, J.; Rinzler, A. G.; Colbert, D.; Smith, K. A.; Smalley, R. E. *Appl. Phys. Lett.* **1999**, *74*, 2307.
(6) Murata, K.; Kaneko, K.; Kanoh, H.; Kasuya, D.; Takahashi, K.; Kokai, F.; Yudasaka, M.; Iijima, S. *J. Phys. Chem. B* **2002**, *106*, 11132.
(7) Anson, A.; Callejas, M. A.; Benito, A. M.; Maser, W. K.; Izquierdo, M. T.; Rubio, B.; Jagiello, J.; Thommes, M.; Parra, J. B.; Martinez, M. T. *Carbon* **2004**, *42*, 1237.
(8) Wang, Q.; Johnson, J. K. *J. Phys. Chem. B* **1999**, *103*, 4809.
(9) Wang, Q.; Johnson, J. K. *J. Phys. Chem. B* **1999**, *103*, 277.
(10) Rzepka, M.; Lamp, P.; de la Casa-Lillo, M. A. *J. Phys. Chem. B* **1998**, *102*, 10894.
(11) Yin, Y. F.; Mays, T.; McEnaney, B. *Langmuir* **2000**, *16*, 10521.
(12) Williams, K. A.; Eklund, P. C. *Chem. Phys. Lett.* **2000**, *320*, 352.
(13) Wang, Q.; Johnson, J. K.; Broughton, J. Q. *J. Chem. Phys.* **1997**, *107*, 5108.
(14) Wang, Q.; Johnson, J. K. *J. Chem. Phys.* **1999**, *110*, 577.
(15) Challa, S. R.; Sholl, D. S.; Johnson, J. K. *Phys. Rev. B* **2001**, *63*, 245419.
(16) Challa, S. R.; Sholl, D. S.; Johnson, J. K. *J. Chem. Phys.* **2002**, *116*, 814.
(17) Darkrim, F.; Levesque, D. *J. Chem. Phys.* **1998**, *109*, 4981.
(18) Darkrim, F.; Aoufi, A.; Levesque, D. *Mol. Simul.* **2000**, *24*, 51.
(19) Darkrim, F.; Levesque, D. *J. Phys. Chem. B* **2000**, *104*, 6773.
(20) Feynman, R. P.; Hibbs, A. *Quantum Mechanics and Path Integrals*; McGraw-Hill: New York, 1965.
(21) Feynman, R. P. *Statistical Mechanics*; Benjamin: New York, 1972.

that predicted by classical simulations and that quantum effects contribute 15−20% of the amount adsorbed at 77 K. It thus seems that quantum effects on the adsorption of hydrogen must be taken into account not only below 77 K but also at room temperature when the adsorption site is in a pore whose size is comparable to that of a hydrogen molecule.

The FH effective potential, which is the $\hbar^2$-Taylor expansion of the original Gaussian FH potential, can be used when systems are under usual densities and $\lambda_B^* \leq 0.5$ ($\lambda_B^* = \hbar/(mk_BT\sigma^2)^{1/2}$, where m and σ are the mass and size of the fluid molecule, respectively, and k_B is the Boltzmann constant.[22,23] The λ_B^* value for hydrogen at 77 K is 0.47, so when hydrogen adsorption above 77 K is considered, the FH method should give a result identical to that given by the rigorous path integral method.[21] The FH method is also of great advantage for simulating quantum fluid systems (at appropriate densities and temperatures) because the potential energy calculations are not as time-consuming as the calculations required when the path-integral method is used.

Many other theoretical and simulation studies concerning quantum effects on helium and hydrogen adsorption at low temperature have been reported,[24−29] as have experimental studies of the adsorption of helium, hydrogen, deuterium, and neon quantum fluids.[30−37] In few studies, however, have experimental results been compared with the predictions of simulations and theoretical studies including quantum effects. It is therefore important to examine how the results of quantum simulations of the adsorption for quantum fluids such as hydrogen isotopes on SWNTs agree with the results of experimental studies. Experimental results obtained with ordinary SWNTs are hard to compare with theoretical results because ordinary SWNTs are contaminated with metal catalysts and amorphous carbon. Single-wall carbon nanohorns (SWNHs),[38−42] however, are free of such impurities and are thus suitable for studying quantum effects appearing in the adsorption of hydrogen isotopes. Iijima et al. reported that SWNHs with purity greater than 90% can be produced at room temperature without metal catalysts by CO_2 laser ablation of pure graphite under argon at atmospheric pressure.[38] A SWNH is typically a tube 2−6 nm in diameter and 40−50 nm long and has a conical cap at one end. SWNHs associate with each other and form a nanoporous Dahlia-flowerlike assembly 80−100 nm in diameter. Because several grams of high-purity SWNHs can be produced easily, the physical adsorption of quantum hydrogen on SWNT-related materials should be investigated by systematically studying the adsorption of hydrogen isotopes on SWNHs.

In this paper, we present adsorption isotherms of H_2 and D_2 on SWNHs at 77 K and study the constitutive properties of quantum fluid adsorption by comparing the H_2 and D_2 adsorption isotherms. We also report the results of GCMC simulations with the FH effective potential (FH-GCMC) for H_2 and D_2 adsorption on SWNTs and SWNHs at 77 K, and we compare the predictions of those simulations with the adsorption measured experimentally.

II. Experimental Section

An as-grown SWNH sample (denoted as-SWNH) was oxidized at 693 K to open nanoscale windows on the wall of the SWNH particle (ox-SWNH). Details of the oxidation method have been provided elsewhere.[41] Adsorption isotherms of H_2 and D_2 at 77 K for the SWNH samples were measured with a laboratory-designed volumetric adsorption equipment[34,36] consisting of a gas-handling system and a cryostat with a He closed-cycle refrigerator. All samples were outgassed at 423 K for 2 h under a pressure below 0.1 mPa before each isotherm measurement. The exact same sample, which was placed in the sample cell, was used for H_2 and D_2 adsorption measurements without replacing for reducing experimental errors. The temperature was kept within ±0.05 K during the adsorption measurements, and thermal transpiration was taken into account by using the empirical equation of Takaishi and Sensui.[43]

III. Potential Models and Simulations

A. Hydrogen−Hydrogen Interaction Potential. In this study, we treat a hydrogen molecule as a structureless spherical particle and, therefore, model the H_2-H_2 interaction by the Lennard-Jones (LJ) potential

$$V_{LJ}(r) = 4\epsilon_{ff}\left[\left(\frac{\sigma_{ff}}{r}\right)^{12} - \left(\frac{\sigma_{ff}}{r}\right)^{6}\right] \quad (1)$$

where r is the distance between two particles. The LJ interaction parameters we used for hydrogen in this work are $\sigma_{ff} = 0.2958$ nm and $\epsilon_{ff}/k = 36.7$ K.[18,19] Here, we use the Feynman−Hibbs (FH) effective potential to introduce quantum corrections to the statistical properties predicted from GCMC simulations with the classical LJ potential. In the FH treatment, a quantum fluid molecule is represented by a Gaussian wave packet of width $\hbar/(12mk_BT)^{1/2}$, so the effective potential can be obtained by averaging the classical LJ potential over the Gaussian. If we expand this Gaussian FH effective potential to the second order, we can obtain the following quadratic FH effective potential:[22,23]

$$V_{FH}(r) = V_{LJ}(r) + \left(\frac{\hbar^2}{24\mu k_BT}\right)\nabla^2 V_{LJ}(r) \quad (2)$$

where $\mu = m/2$ is the reduced mass of a pair of interacting

(22) Sesé, L. M. *Mol. Phys.* **1994**, *81*, 1297.
(23) Sesé, L. M. *Mol. Phys.* **1995**, *85*, 931.
(24) Gatica, S. M.; Stan, G.; Calbi, M. M.; Johnson, J. K.; Cole, M. W. *J. Low Temp. Phys.* **2000**, *120*, 337.
(25) Cole, M. W.; Hernández, E. S. *Phys. Rev. B* **2002**, *65*, 092501.
(26) Stan, G.; Cole, M. W. *J. Low Temp. Phys.* **1998**, *112*, 539.
(27) Wang, Q.; Johnson, J. K. *Mol. Phys.* **1998**, *95*, 299.
(28) Gu, C.; Gao, G.-H. *Phys. Chem. Chem. Phys.* **2002**, *4*, 4700.
(29) Gu, C.; Gao, G.-H.; Yu, Y. X. *J. Chem. Phys.* **2003**, *119*, 488.
(30) Setoyama, N.; Kaneko, K. *Adsorption* **1995**, *1*, 165.
(31) Stéphanie-Victorie, F.; Goulay, A.-M.; Cohen de Lara, E. *Langmuir* **1998**, *14*, 7255.
(32) Teizer, W.; Hallock, R. B.; Dujardin, E.; Ebbesen, T. W. *Phys. Rev. Lett.* **1999**, *82*, 5305; **2000**, *21*, 1844.
(33) Day, C. *Colloids Surf., A* **2001**, *187−188*, 187.
(34) Tanaka, H.; El-Merraoui, M.; Kodaira, T.; Kaneko, K. *Chem. Phys. Lett.* **2002**, *351*, 417.
(35) Tanaka, H.; Murata, K.; Miyawaki, J.; Kaneko, K.; Kokai, F.; Takahashi, K.; Kasuya, D.; Yudasaka, M.; Iijima, S. *Mol. Cryst. Liq. Cryst.* **2002**, *388*, 429.
(36) Tanaka, H.; El-Merraoui, M.; Kanoh, H.; Steele, W. A.; Yudasaka, M.; Iijima, S.; Kaneko, K. *J. Phys. Chem. B* **2004**, *108*, 17457.
(37) Wilson, T.; Tyburski, A.; DePies, M. R.; Vilches, O. E.; Becquet, D.; Bienfait, M.; *J. Low Temp. Phys.* **2002**, *126*, 403.
(38) Iijima, S.; Yudasaka, M.; Yamada R.; Bandow, S.; Suenaga, K.; Kokai, F.; Takahashi, K. *Chem. Phys. Lett.* **1999**, *309*, 165.
(39) Murata, K.; Kaneko, K.; Steele, W. A.; Kokai, F.; Takahashi, K.; Kasuya, D.; Yudasaka, M.; Iijima, S. *Nano Lett.* **2001**, *1*, 197.
(40) Ohba, T.; Murata, K.; Kaneko, K.; Steele, W. A.; Kokai, F.; Takahashi, K.; Kasuya, D.; Yudasaka, M.; Iijima, S. *Nano Lett.* **2001**, *1*, 371.
(41) Murata, K.; Kaneko, K.; Steele, W. A.; Kokai, F.; Takahashi, K.; Kasuya, D.; Hirahara, K.; Yudasaka, M.; Iijima, S. *J. Phys. Chem. B* **2001**, *105*, 10210.
(42) Bekyarova, E.; Murata, K.; Yudasaka, M.; Kasuya, D.; Iijima, S.; Tanaka, H.; Kanoh, H.; Kaneko K. *J. Phys. Chem. B* **2003**, *107*, 4681.
(43) Takaishi, T.; Sensui, Y. *Trans. Faraday Soc.* **1963**, *53*, 2503.

fluid molecules. The potential parameters for H_2 and D_2 are identical, so that the difference in properties of these quantum fluids is due solely to the difference in molecular mass. In other words, it is due to the difference in quantum effects.

B. Hydrogen−SWNT Interaction Potential. For simplicity, we assumed that a SWNT can be modeled as an infinitely long cylindrical tube with a smooth wall. The solid−fluid interaction potential based on the classical LJ potential inside such a tube can be calculated by integrating the pairwise LJ potential (eq 1) over the infinitely long tube, and that integral is given by[44]

$$V_{\mathrm{LJ}}^{\mathrm{tube}}(r,R) = \pi^2 \rho_s \epsilon_{sf} \sigma_{sf}^2 \left[\frac{63}{32} \frac{F(-4.5, -4.5, 1.0; r^{*2})}{[R^*(1-r^{*2})]^{10}} - 3 \frac{F(-1.5, -1.5, 1.0; r^{*2})}{[R^*(1-r^{*2})]^{4}} \right] \quad (3)$$

where $F(\alpha, \beta, \gamma; \chi)$ is a hypergeometric function; R is the radius of the tube; ρ_s is the density of solid atoms in the tube wall (38.2 nm^{-2} in a SWNT); $r^* = r/R$, and $R^* = R/\sigma_{sf}$. The interaction parameters we used for the hydrogen−SWNT interaction are $\sigma_{sf} = 0.3179$ nm and $\epsilon_{sf}/k = 32.06$ K. They were obtained by using the Lorentz−Berthelot rules and combining the parameters for graphite ($\sigma_{ss} = 0.34$ nm and $\epsilon_{ss}/k = 28.0$ K) with those for hydrogen. The quantum hydrogen−SWNT interaction potential, obtained by integrating the pairwise FH effective potential (eq 2), is given by

$$V_{\mathrm{FH}}^{\mathrm{tube}}(r,R) = V_{\mathrm{LJ}}^{\mathrm{tube}}(r,R) + \pi^2 \rho_s \epsilon_{sf} \left(\frac{\hbar^2}{m k_B T} \right) \left[\frac{2541}{256} \frac{F(-5.5, -5.5, 1.0; r^{*2})}{[R^*(1-r^{*2})]^{12}} - \frac{25}{8} \frac{F(-2.5, -2.5, 1.0; r^{*2})}{[R^*(1-r^{*2})]^{6}} \right] \quad (4)$$

where instead of using the $\mu = m/2$, we used for the H_2−H_2 interaction; we used $\mu = m$ for the quantum interaction between hydrogen and carbon atoms because we assumed that the carbon atoms in the SWNT wall are linked together rigidly.

C. Hydrogen−SWNH Interaction Potential. In the present study, a SWNH was modeled by a SWNT-like tube with a conical cap at each end. These two caps were used to avoid cutting off of the intermolecular interactions discontinuously when terminating the one end of the SWNH model. The tubular part and one conical cap of the SWNH model are shown in Figure 1a, together with a TEM image of SWNH (Figure 1b). The tube and the base of the cone of the SWNH model are 2 nm in diameter, and the lengths of the cone and tube are 5.9 and 2.958 nm (10 σ_{ff}), respectively. The angle of the apex of the cone was set to 19° from the TEM observations. We made the length of the tubular part of the SWNH model less than a tenth the length of the actual SWNHs because we wanted to evaluate adsorption behaviors of the hydrogen isotopes around the conical parts of SWNHs. Each conical part of the SWNH model consists of a graphite layer one atom thick rolled into a cone. Thus, as shown in Figure 1a, it also has an atomistic structure. The interaction potential between a quantum hydrogen and a carbon atom in the conical wall were calculated by assuming $\mu = m$ and using eq 2, but the structureless model was used for the tubular part of the SWNH model and the potential contribution from the quantum hydrogen−tube wall interaction was calculated using eq 4, which was multiplied by a polynomial function to account for the finite length of the tubular part of the SWNH model. The polynomial function was fitted so that the [quantum hydrogen]−[tube wall] interaction inside the SWNH model reproduced the potential profile for a SWNT of finite length. Thus, along the tube axis, the [quantum hydrogen]−[tube wall] interaction was continuously reduced from near the connection between the tube and cone parts to the inside of the cone part.

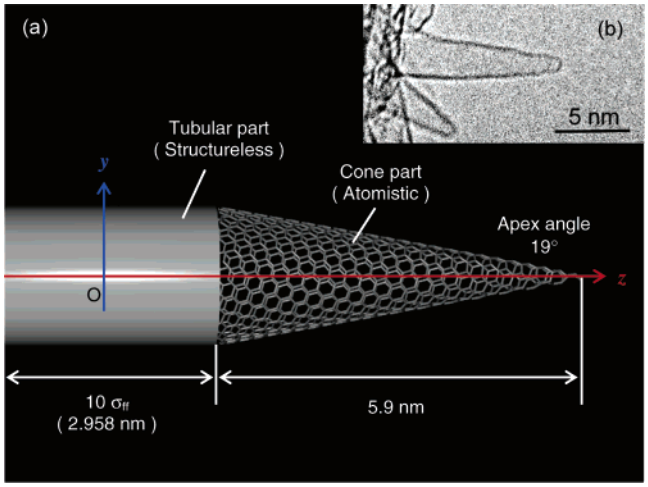

Figure 1. Schematic representation of the SWNH model used for the FH-GCMC simulations; only one conical part of the SWNH model is shown (a) and the TEM image of SWNH (b).

D. Isosteric Heat of Adsorption. To evaluate the solid−fluid interaction potentials of the SWNH model, we calculated the isosteric heat of adsorption (q_{st}) from the fluctuations in the number of adsorbed molecules and the total energy:[27]

$$q_{st} = \frac{2}{5} k_B T - \frac{\langle EN \rangle - \langle E \rangle \langle N \rangle}{\langle N^2 \rangle - \langle N \rangle^2} \quad (5)$$

where the total energy E is the sum of the kinetic and potential energies. The total energy based on the FH model is given by

$$E = \frac{3}{2} N k_B T + \sum_{i<j}^{N} \beta \frac{dV_{\mathrm{FH},ij}^{\mathrm{ff}}}{d\beta} + \sum_{i}^{N} \beta \frac{dV_{\mathrm{FH},i}^{\mathrm{sf}}}{d\beta} + \sum_{i<j}^{N} V_{\mathrm{FH},ij}^{\mathrm{ff}} + \sum_{i}^{N} V_{\mathrm{FH},i}^{\mathrm{sf}} \quad (6)$$

where $V_{\mathrm{FH}}^{\mathrm{ff}}$ and V_{FH}^{sf} are the fluid−fluid and solid−fluid interaction potentials, respectively, based on the FH effective potential; N is the number of adsorbed molecules in the system, and $\beta = 1/k_B T$. The first term on the right-hand side of eq 6 is the kinetic energy of classical molecules; the second and third terms are quantum corrections to the classical kinetic energy, and the rest of the terms are the potential energies.

E. Simulation Details. The grand canonical Monte Carlo method[45] based on the FH effective potential (FH-GCMC) was used to simulate quantum H_2 and D_2 adsorption at 77 K. The probabilities of a single displacement, creation, and deletion were set to 0.4, 0.3, and 0.3, respectively. The system was

(44) Tjatjopoulos, G. J.; Feke, D. L.; Mann, J. A., Jr. *J. Phys. Chem.* **1988**, *92*, 4006.

(45) Allen, M. P.; Tildesley, D. J. *Computer Simulation of Liquids*; Clarendon Press: Oxford, 1987.

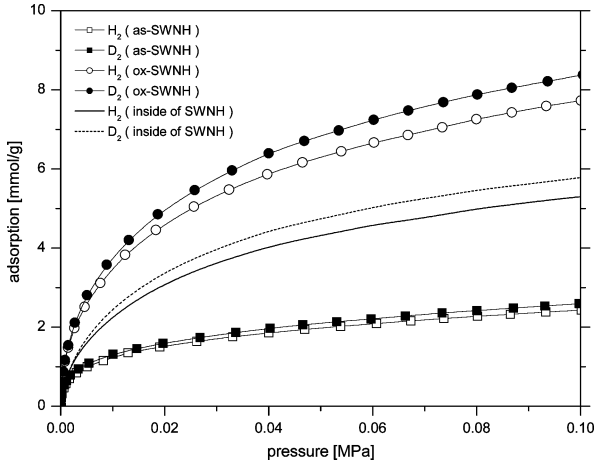

Figure 2. H_2 and D_2 adsorption isotherms for as-SWNH, ox-SWNH, and the internal space of SWNH at 77 K.

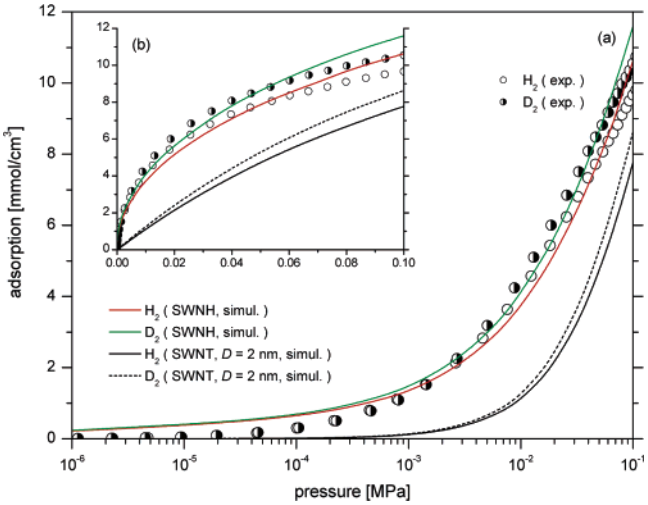

Figure 3. H_2 and D_2 adsorption isotherms at 77 K. The circles represent the experimental values for the internal space of SWNH. The four lines are predictions from the FH-GCMC simulations for the SWNH and SWNT models.

equilibrated for 5×10^6 Monte Carlo steps, after which data were collected for another 5×10^6 steps. The fluid−fluid and solid−fluid (for the atomistic cone parts of the SWNH model) interactions were truncated at distances of 5 σ_{ff} and 5 σ_{sf}, respectively. We have calculated the adsorption of H_2 and D_2 in the internal space of the SWNT model (the tube diameter is 2 nm) and the SWNH model (the diameters of the tube and the base of the cone are 2 nm). Periodic boundary conditions were not used for the SWNH model but were used for the SWNT model, and there only along the tube axis. Thus the tube length of 10 σ_{ff} was used. The simulations yield an absolute amount adsorbed (N_{abs}), and thus it must be converted to a surface excess (N_{exc}) for comparison with experimental data. In the present study, the surface excess has been calculated by $N_{exc} = N_{abs} - \rho_b V$, where ρ_b is the bulk density of gas, and V is the volume of the internal space of the SWNH model. In the grand canonical ensemble, the volume, temperature, and adsorbate chemical potential are fixed. To compare with experimental isotherms as a function of a bulk fluid pressure, however, we need to obtain the pressure of the bulk fluid as a function of the chemical potential and temperature. Therefore, to determine the excess chemical potentials of the quantum hydrogen isotopes at 77 K, we performed Monte Carlo simulations with the FH effective potential in the canonical ensemble (FH-MC), which is combined with the Widom test particle insertion method.[46] The pressures of the quantum hydrogen isotopes were calculated simultaneously during the FH-MC simulations. We also obtained the pressure of bulk quantum hydrogen as a function of density from the FH-MC simulations at 78 K and confirmed that the results are in good agreement with experimental data up to at least 10 MPa.

IV. Results and Discussion

H_2 and D_2 adsorption isotherms at 77 K for as-SWNH, ox-SWNH, and the inside of SWNH are shown in Figure 2. The isotherms for adsorption inside the SWNH were obtained by subtracting the isotherms for adsorption on as-SWNH from the isotherms for adsorption on ox-SWNH. Differences in adsorption between H_2 and D_2 are 6% for as-SWNH, 7% for ox-SWNH, and 8% for the inside of SWNH, and those differences are constant to within ±2% deviation over the pressure range from 0.007 to 0.1 MPa. The ratio of the λ_B^* value for H_2 to that for D_2 is 1.4, so the quantum correction (the second term on the right-hand side of eq 2) to the interaction potential for H_2 is twice as large as that to the interaction potential for D_2. As a consequence, for example, the potential well depth of the H_2-H_2 interaction at 77 K calculated from eq 2 is 1.8 K shallower than that of the D_2-D_2 interaction and is 4.4 K shallower than that of the classical H_2-H_2 interaction (LJ potential). Similarly, the potential well depth of the H_2−SWNT ($D = 2$ nm) interaction at 77 K calculated from eq 4 is 10 K shallower than that of the D_2−SWNT interaction and 22 K shallower than that of the classical H_2−SWNT interaction calculated from eq 2. These quantum contributions would result in the difference between the amounts of H_2 and D_2 adsorbed on the SWNH samples.

We have performed the FH-GCMC simulations for H_2 and D_2 adsorption at 77 K on the SWNH model and also the model of SWNT, which is 2 nm in diameter. The simulated adsorption isotherms at 77 K are shown in Figure 3a,b, together with the experimental isotherms for the H_2 and D_2 adsorption inside SWNH. The adsorbed amount from the experimental data has been converted to that on a volumetric basis by using the internal pore volume of SWNH (0.55 cm^3/g) obtained by nitrogen adsorption at 77 K.[36] Although the experimental data indicate that the uptake of the hydrogen isotopes increases rapidly up to about 0.01 MPa, the predictions from the FH-GCMC simulations for the SWNT model do not reproduce this rapid increase (see Figure 3b). The simulated H_2 and D_2 adsorption isotherms for the SWNH model are in reasonably good agreement with the experimental data over a wide range of pressures, although this SWNH model is quite simplified in comparison with the actual SWNH. Some configurational snapshots collected during the simulations for hydrogen adsorption in the SWNH model are shown in Figure 4a−d, and it is clear from these snapshots that the rapid rise in the adsorption isotherms up to about 0.01 MPa can be attributed to adsorption in the conical part of the SWNH model. These facts indicate that at 77 K and pressures below 0.1 MPa most of the hydrogen isotopes are preferentially concentrated in the conical part of

(46) Widom, B. *J. Chem. Phys.* **1963**, *39*, 2802.

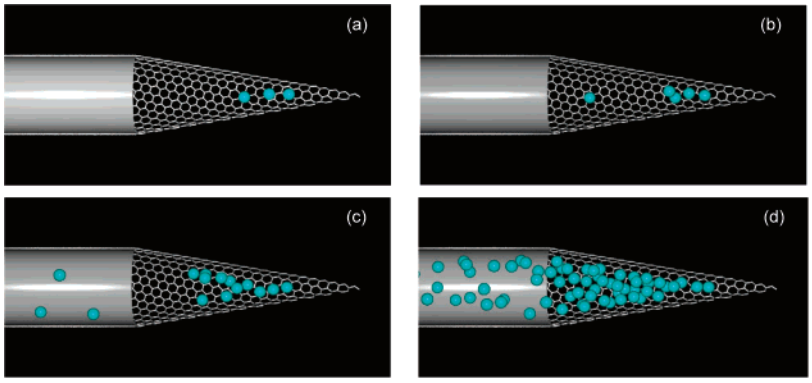

Figure 4. Configurational snapshots collected from the FH-GCMC simulations for H_2 adsorption in the SWNH model at 77 K; (a) 10^{-4} MPa, (b) 10^{-3} MPa, (c) 10^{-2} MPa, and (d) 0.1 MPa.

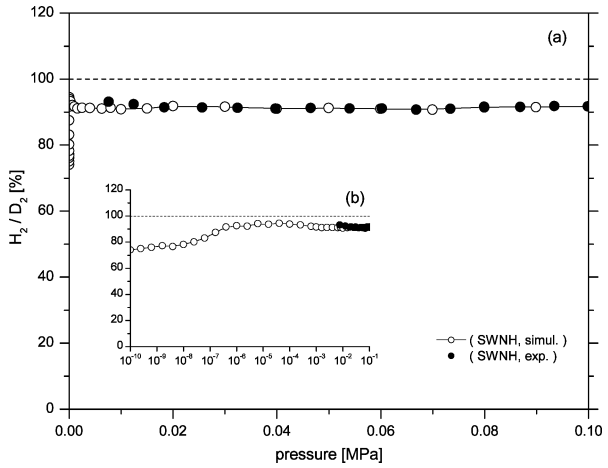

Figure 5. Relation between pressure and the ratio of H_2 adsorption to D_2 adsorption in the internal space of SWNH at 77 K.

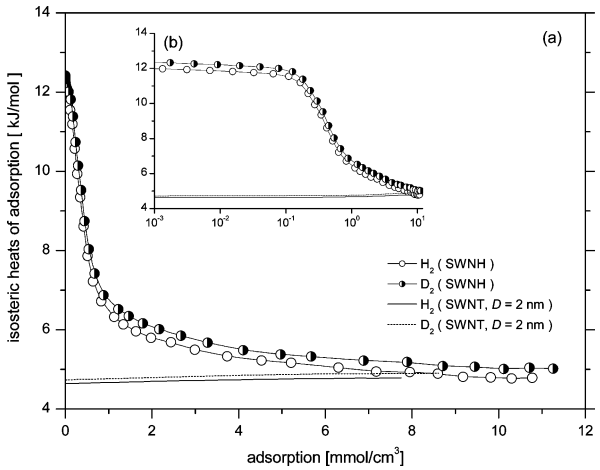

Figure 6. Simulated isosteric heats for H_2 and D_2 in the SWNH and SWNT models versus the average amounts adsorbed at 77 K.

SWNH, which is less than 2 nm in diameter, because of the strong solid−fluid interaction potential field there.

To discuss the agreement between the predictions from the FH-GCMC simulations for the SWNH model and the experimental data with respect to quantum effects, we have calculated the ratio of H_2 adsorption to D_2 adsorption from the simulations and the experimental data and plotted it as a function of pressure in Figure 5. The H_2/D_2 ratios obtained from the FH-GCMC simulations agree very well with the experimental results over the pressure range from 0.007 to 0.1 MPa. This suggests that quantum effects at 77 K are represented in the FH-GCMC simulations. The H_2/D_2 ratio obtained from the FH-GCMC simulations is 92 ± 2% over the range of pressures from 10^{-6} to 0.1 MPa and decreases to about 74% at 10^{-10} MPa. Below 10^{-7} MPa, most hydrogen isotopes are adsorbed only at the tip of the conical part of the SWNH model, where only one adsorbate molecule can be accommodated. The large difference in adsorption between H_2 and D_2 at low pressures should therefore be attributed to significant quantum effects. That is, it is harder for a H_2 molecule to approach the tip of the SWNH model, which has the strongest potential field, than it is for a D_2 molecule because of the wide quantum spreading of a H_2 molecule (proportional to $\hbar/(6mk_BT)^{1/2}$). We have also performed additional simulations of the classical LJ hydrogen adsorption at 77 K in the SWNH model without quantum corrections. The density of adsorbed hydrogen predicted by the quantum simulation is 81 ± 1% of that predicted by the classical simulation over the pressure range from 0.001 to 0.1 MPa, and it is only about 52% of that predicted by the classical simulation at 10^{-10} MPa. We have calculated the isosteric heat of adsorption (q_{st}) for the hydrogen isotopes in the SWNH model at 77 K, and the values obtained from the FH-GCMC simulations for the SWNH and SWNT (D = 2 nm) models are shown in Figure 6a,b as a function of average amounts adsorbed. At zero coverage, the isosteric heats of adsorption for H_2 on the SWNH model are nearly 3 times as large as that on the SWNT model because of the strong solid−fluid interaction potential at the tip of the SWNH model. Then the q_{st} values for the respective hydrogen isotopes on the SWNT model are almost constant over the full range of adsorption, while the q_{st} values for the SWNH model show a sharp decrease in q_{st} from 0.2 to about 2 mmol/cm^3. The reason for the decrease in q_{st} with an increase in amounts adsorbed is that the solid−fluid interaction in the conical part decreases rapidly from the tip of the cone to the connection between the conical part and the tube part. That is, molecules adsorbing after occupation of strong adsorption sites by other molecules experience a smaller solid−fluid interaction potential. This is also evident from the fact that the q_{st} values for the SWNH model approach those for the SWNT model after completion of filling in the conical part of the SWNH model. The q_{st} for H_2 is always smaller than that for D_2, and at zero coverage, the difference in q_{st} between H_2 and D_2 for the SWNH model is 0.35 kJ/mol, while for the SWNT model, it is 0.09 kJ/mol. This clearly indicates that the smaller the pore size, the larger the quantum effects on the adsorption of hydrogen isotopes. We have also estimated the quantum contribution to

q_{st} at zero coverage for H_2 on the SWNH model by comparing the prediction from the quantum simulation with that from the classical simulation. The q_{st} value for classical H_2 at zero coverage is 0.78 kJ/mol larger than that for quantum H_2 and is about twice as large as the difference between the q_{st} values for quantum H_2 and D_2. These facts thus suggest that quantum effects on hydrogen adsorption for SWNHs are very important at 77 K.

V. Conclusions

We have measured H_2 and D_2 adsorption on SWNHs at 77 K and compared the experiments with the simulations for these hydrogen isotopes adsorption on the SWNH model. Quantum effects were incorporated in the simulations through the Feynman−Hibbs (FH) effective potential. The simulation results are in good agreement with the experimental results, even though the SWNH model is much simpler than the actual SWNHs. The ratio of H_2 adsorption to D_2 adsorption obtained from the FH-GCMC simulations is 92 ± 2% over the pressure range of 0.007−0.1 MPa and shows close agreement with the experimental results. This indicates that quantum effects at 77 K are accurately represented in the FH-GCMC simulations. Moreover, the ratio of quantum H_2 adsorbed to classical H_2 adsorbed approaches 80% over the pressure range of 0.007−0.1 MPa. The difference between the amounts of H_2 and D_2 adsorbed that is predicted by the quantum simulations becomes larger as pressure decreases. This is because the quantum spreading of H_2, which is wider than that of D_2, is quite effective at the narrow conical part of the SWNH model. The q_{st} values for H_2 obtained from the quantum simulations are always smaller than those obtained for D_2. At zero coverage, the q_{st} difference between H_2 and D_2 is 0.35 kJ/mol, and the q_{st} difference between quantum H_2 and classical H_2 is 0.78 kJ/mol. These facts indicate that quantum effects on hydrogen adsorption on SWNHs are very important even at 77 K.

Acknowledgment. This work was partially funded by a Grand-in-Aid for Fundamental Scientific Research (S) (No. 15101003) from the Japanese Government, and by the Advanced Nanocarbon Application Project, NEDO. We would like to thank Jing Fan for TEM observations.

JA0502573